Activation of the TP53 pathway is a therapeutic vulnerability in NUP98::KDM5A^{+} pediatric AML

Luca Nunzio Cifarelli[1,2], Hasan Issa[2], Ludovica Proietti[6], Konstantin Schuschel[2], Lucie Gack[3], Katja Menge[3], Christian Ihling[4,5], Meike Vogler[1], Andrea Sinz[4,5], Jan-Henning Klusmann[2*], Dirk Heckl[1,2*]

[1] Institute for Experimental Pediatric Hematology and Oncology, Goethe-University Frankfurt, Frankfurt am Main, Germany

[2] Dep. of Pediatrics, Goethe-University Frankfurt, Frankfurt am Main, Germany

[3] Dep. of Pediatric Hematology and Oncology, Martin-Luther-University Halle-Wittenberg, Halle, Germany

[4] Dep. of Pharmaceutical Chemistry and Bioanalytics, Martin-Luther-University Halle-Wittenberg, Halle, Germany

[5] Center for Structural Mass Spectrometry, Martin-Luther-University Halle-Wittenberg, Halle, Germany

[6] Centre of Biological Sciences, University of Veterinary Medicine, Vienna, Austria

*authors contributed equally to the work

Correspondence: Dirk Heckl, Institute for Experimental Pediatric Hematology and Oncology, Goethe-University Frankfurt, Komturstraße 3a, 60528 Frankfurt am Main, Germany; e-mail: heckl@med.uni-frankfurt.de.

Disclosures: J-HK has advisory roles for Boehringer, Roche and Jazz Pharmaceuticals. All other authors declare that the manuscript was written in the absence of any commercial or financial relationships that could be perceived as a potential conflict of interest.

Graphical abstract

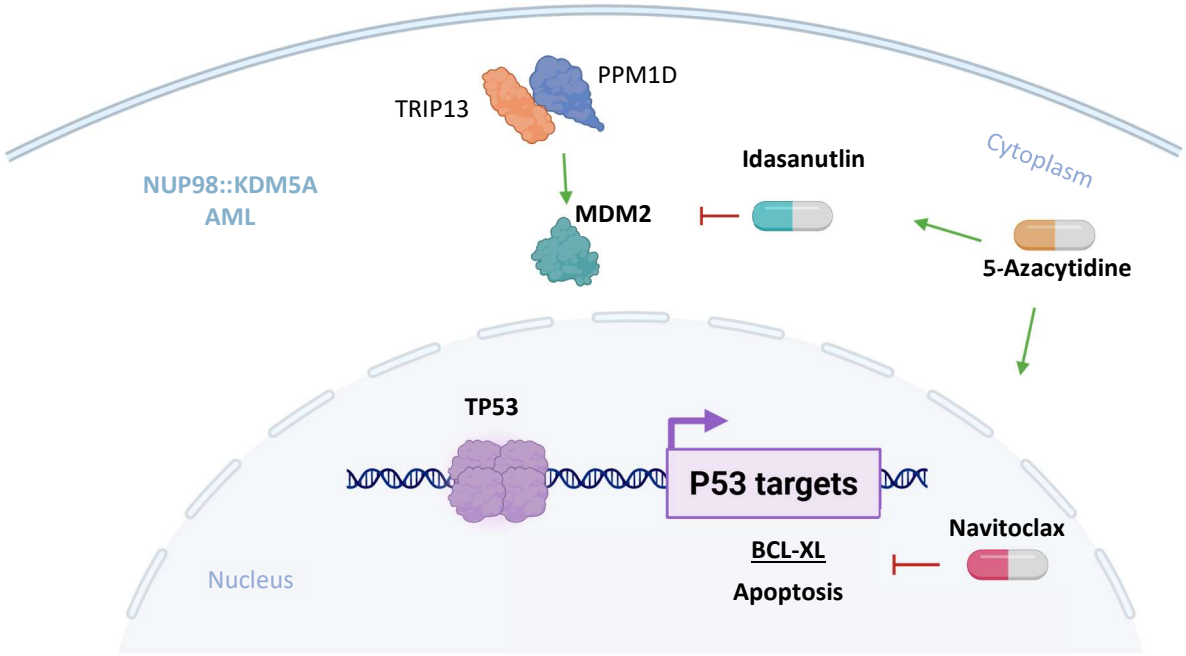

Abstract

Pediatric acute myeloid leukemia (AML) driven by the NUP98::KDM5A fusion is an aggressive subtype predominantly arising in infancy, with limited therapeutic options and poor prognosis. Using matched fetal and adult hematopoietic stem and progenitor cell models, we demonstrate that NUP98::KDM5A-driven leukemia originating in a fetal context exhibits enhanced aggressiveness and sustains fetal-specific transcriptional programs. Functional genomic and proteomic analyses identified a critical dependency on the AAA^{+} ATPase TRIP13, which binds the phosphatase PPM1D to suppress TP53 activation. Pharmacologic inhibition of TRIP13 or combined treatment with idasanutlin, navitoclax, and 5-azacytidine—three clinically approved agents—effectively reactivated TP53 signaling and induced synergistic apoptosis in a synergistic manner in NUP98::KDM5A AML models. These findings reveal a developmentally regulated TRIP13/PPM1D–TP53 survival axis that can be exploited for targeted therapy, offering

a mechanistically grounded and translatable strategy to improve outcomes for this high-risk pediatric leukemia patients.

Introduction

Pediatric acute myeloid leukemia (AML) is a heterogenous disease, accounting for ~15-20% of all pediatric acute leukemias, and its mutational landscape substantially differs from that of adult AML even within different pediatric age groups [1-5]. The different subgroups and the distinct mutations occurring in pediatric AML may in part be attributable to the ontogeny and the cellular environment, which is particularly prominent in infant AML (≤2 years of age) [6-8]. Indeed, in some instances, oncogenic driver mutations have been detected at birth pointing to an *in utero* origin of the disease that is linked with fetal hematopoiesis [9, 10]. While definitive proof is still missing, an association of the molecular properties of fetal cells and their environment may explain the high prevalence of certain chromosomal translocations and subgroups.

One of these highly prevalent subgroups is acute megakaryoblastic leukemia (AMKL), which is an aggressive form of AML associated with lower event-free and overall survival in the absence of underlying Down syndrome (trisomy 21) and occurs in up to 15% of AML children [11-13].

A main genetic driver event in AMKL is the chromosomal translocation t(11;12), which generates the NUP98::KDM5A fusion oncoprotein composed of the N- terminal glycine-leucine-phenylalanine-glycine (GLFG) repeat motif of NUP98 and the C-terminal plant homeodomain finger (PHD3) of histone lysine demethylase KDM5A (also known as JARID1A) [14, 15].

Several studies have shown that *NUP98::KDM5A* drives transformation of murine hematopoietic stem and progenitors cells (HSPCs) and recapitulates the principal aspect of the disease, such as the transcriptional upregulation of *HOXA* and *HOXB*

gene clusters [16-18]. However, in contrast to *CBFA2T3::GLIS2* or *KMT2A*-rearranged AML [6], the impact and the molecular role of the fetal origin in disease onset have not yet been studied for NUP98::KDM5A.

Fetal and adult hematopoiesis differ in various important aspects [19, 20]. First of all, cellular composition of fetal liver hematopoiesis is vastly different from the adult bone marrow with a skewing for erythro-megakaryocytic output [9, 21]. More importantly, fetal hematopoietic stem cells are highly proliferative and self-renewing when building the stem cell pool for lifelong support of blood formation, whereas the adult counterparts are quiescent to maintain genomic integrity [21-23]. Molecularly, these distinctions are coordinated by diverging epigenetic – and resulting transcriptional – programs. Notably, the majority of the chromosomal translocations detected in infant AML affect epigenetic regulators [24].

Here, we show that fetal ontogeny contributes to the aggressiveness of NUP98::KDM5A AML in part by sustaining a TRIP13/PPM1D-TP53 survival axis, and we exploit this vulnerability through direct TRIP13 inhibition or a readily translatable idasanutlin–navitoclax–5-azacytidine combination.

Results

NUP98::KDM5A induces aggressive leukemia in fetal HSPCs

To identify the impact of ontogeny in NUP98::KDM5A-driven leukemia, we generated matched fetal and adult murine cell models for NUP98::KDM5A AML. Murine Hematopoietic Stem and Progenitor Cells (HSPCs) were isolated from fetal liver of healthy fetuses at E13.5 (mFL-HSPCs) and from bone marrow of adult mice (mBM-HSPCs) and then transduced with a lentiviral vector expressing the human NUP98::KDM5A cDNA[25] and EGFP (Fig. 1a). Both adult and fetal cells showed a

progressive outgrowth of NUP98::KDM5A$^+$ GFP$^+$ cells indicative of transformation, whereas control vector transduced cells exhausted over time (Fig. 1b and Supplementary Fig. 1a). Despite comparable transduction rates and similar immunophenotype, fetal NUP98::KDM5A$^+$ cells outcompeted the untransduced HSPCs significantly faster than the adult NUP98::KDM5A$^+$ cells (Fig. 1b and Supplementary Fig. 1a).

Immunophenotypic analysis revealed that NUP98::KDM5A expression maintained cells in an immature LSK (Lineage$^-$ c-Kit$^+$ Sca1$^+$) state with maturation arrest, corroborated by cytology (Fig. 1c-d and Supplementary Fig. 1b) and transcriptional profiling (Supplementary Fig. 1c). CIBERSORT [26, 27] deconvolution of bulk RNA-seq revealed that fetal NUP98::KDM5A cells showed a significantly higher proportion of immature progenitors relative to control cells —an effect not observed in the adult counterpart (Fig. 1e and Supplementary Table 3). Gene expression analysis confirmed that fetal NUP98::KDM5A$^+$ cells retained fetal signatures compared to adult cells (Fig. 1f). As expected, both models exhibited upregulation of *HOXA* and *HOXB* gene clusters and marked downregulation of *RB1* target genes (Supplementary Fig. 1c and Supplementary Table 5), consistent with a transcriptional program resembling the RB1-mutant state frequently co-occurring in NUP98::KDM5A AML [12, 15, 28].

In vivo, transplantation of fetal NUP98::KDM5A$^+$ cells into syngeneic recipients resulted in significantly accelerated leukemia development compared to adult-derived cells (latency fetal: 36 days; adult: 70 days; median disease-free survival; $P_{log\ rank}$ =1.068e-005; Fig. 1g). Splenomegaly was significantly more pronounced in mice receiving fetal NUP98::KDM5A$^+$ cells (Fig. 1h). Leukemic blasts in the bone marrow expressed high levels of the mature myeloid surface marker Gr-1 and CD11b (Mac-1), alongside a residual immature LSK fraction (Supplementary Fig. 1d-e).

Our results thus highlight that ontogeny is a key determinant of the aggressivity of NUP98::KDM5A driven AML.

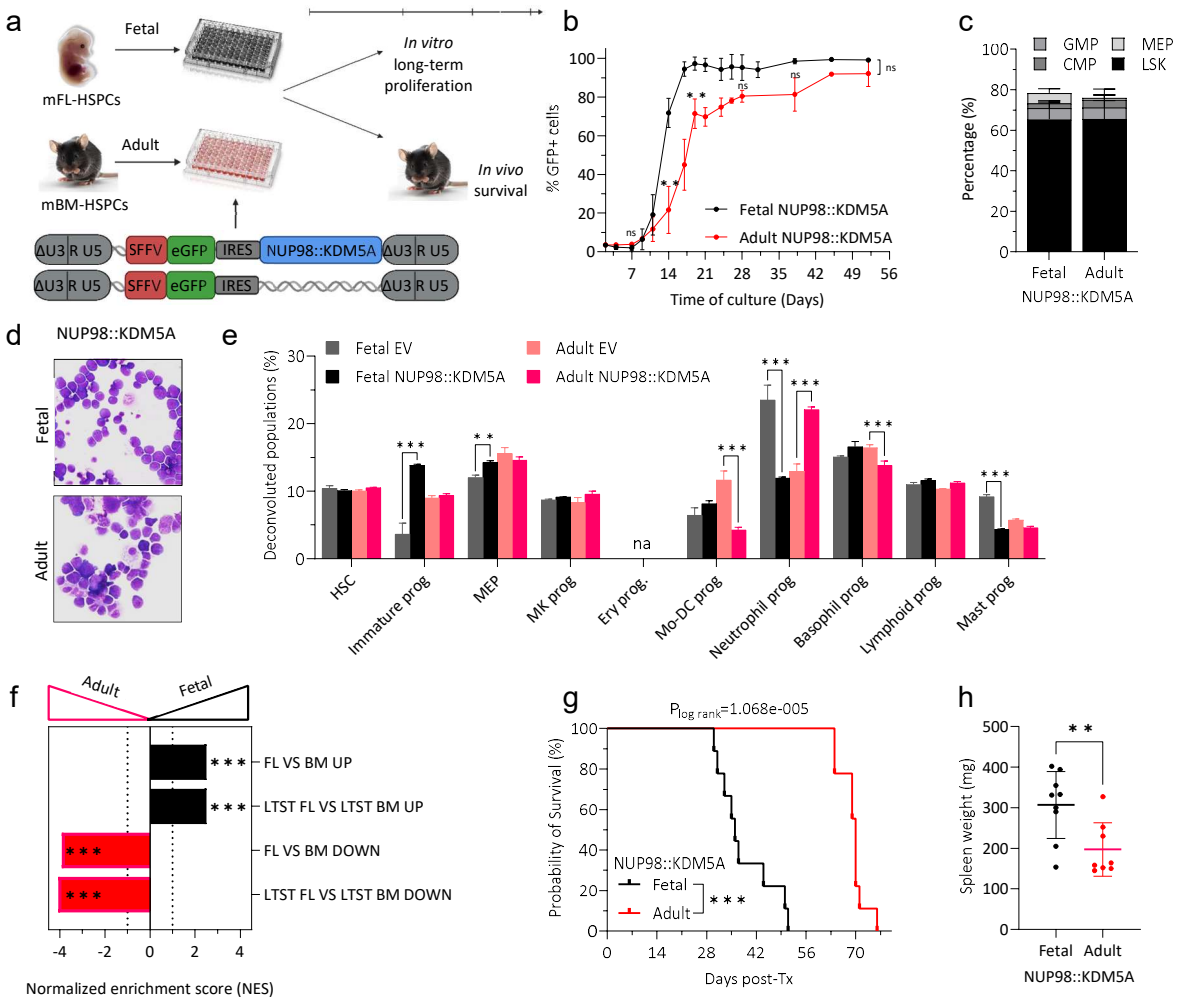

Fig. 1. NUP98::KDM5A fusion protein induces a more aggressive disease in fetal cells.

a) Schematic workflow for the generation of *in vitro* and *in vivo* murine models of constitutive overexpression of NUP98::KDM5A fusion oncoprotein in murine Hematopoietic Stem and Progenitor Cells (HSPCs) isolated from fetal liver (mFL-HSPCs) of healthy fetuses at E13.5 and bone marrow of adult mice (mBM-HSPCs). Created in Biorender.com

b) GFP+ percentage of fetal and adult NUP98::KDM5A^{+} cells maintained in liquid culture. Data from 1 representative experiment performed in replicates (n > 3) are shown as mean s.d. (t-test).

c) Bar graph showing the percentage of LSK (Lineage negative, c-kit+ and Sca1+), Megakaryocytic-erythroid (MEP; Lineage negative, c-kit+, Sca1-, CD16/CD32- and CD34+) and common myeloid (CMP; Lineage negative, c-kit+, Sca1-, CD16/CD32- and CD34-) and granulocyte/monocyte (CMP; Lineage negative, c-kit+, Sca1-, CD16/CD32+ and CD34+) progenitors of fetal and adult NUP98::KDM5A^{+} cells after 4 weeks of culture. (mean ± s.d., n > 3).

d) Representative cytospin images (x40 original magnification) of fetal and adult NUP98::KDM5A$^+$ cells from *in vitro* culture at day 21.
e) Cellular component of bulk RNA samples (n= 3 per condition) inferred by CIBERSORT using signature matrix derived from reference scRNAseq data. Abbreviations. HSC: hematopoietic stem cell, Immature prog: Immature progenitor, MEP: Megakaryocyte–erythroid progenitor, MK prog: Megakaryocyte progenitor, Ery prog: Erythroid progenitor, Mo-DC: Monocyte and Dendritic cell progenitor, Neutrophil prog: Neutrophil progenitor, Basophil prog: Basophil progenitor, Lymphoid prog: Lymphoid progenitor, Mast progenitor: Mastocyte progenitor.
f) Bar graphs showing the normalized enrichment scores (NES) of significantly upregulated or downregulated gene sets in fetal NUP98::KDM5A$^+$ cells compared to adult NUP98::KDM5A$^+$ cells.
g) Kaplan-Meier survival curves of C57BL/6N mice transplanted with fetal and adult NUP98::KDM5A$^+$ cells (n ≥ 6).
h) Dot plot showing spleen weights of C57BL/6N mice injected with fetal and adult NUP98::KDM5A$^+$ cells (mean ± s.d., n ≥ 6) (t-test).

ns, not significant * P < .05, ** P < .01, ***P < .001, ****P < .0001

Fetal dependency screening reveals TRIP13 as a critical vulnerability in NUP98::KDM5A$^+$ AML

The aggressive phenotype of fetal-derived NUP98::KDM5A leukemia is closely linked to the persistence of fetal transcriptional programs. These programs create a developmental vulnerability in the post-fetal hematopoietic environment of pediatric patients, where they may be essential for leukemic maintenance and exploitable for therapeutic intervention. To address this, we performed a CRISPR-Cas9 loss of function screen targeting 867 genes upregulated in human fetal liver HSPCs compared to their adult counterparts [29] in fetal and adult NUP98::KDM5A$^+$ cells (Fig. 2a-b). To achieve selectivity, we complemented the screens with two additional murine AML models – familial-platelet disorder with loss of *Runx1* and *Bcor* (FPD-AML) [30], and myeloid leukemia in Down syndrome (ML-DS) (Fig. 2c and Supplementary Fig. 2a) [31-33]. Applying a depletion cutoff of >70% identified seven candidates, but only the AAA+ (ATPases Associated with diverse cellular Activities) ATPase, *Trip13* also exceeded a fetal/adult ratio of >2.5, highlighting it as a particularly compelling and druggable target (Fig. 2d and Supplementary Fig. 2b). We next validated *Trip13* loss in a single-well fluorescence-based depletion assay with a set of independent gRNAs

(Fig. 2d). To corroborate our findings in the context of human leukemia, we knocked out *TRIP13* using the CRISPR-Cas9 system in a broad variety of human leukemic and non-leukemic (HT1080) cell lines, as well as in primary human fetal HSPCs expressing NUP98::KDM5A. Consistent with murine results, TRIP13 loss markedly impaired the growth of NUP98::KDM5A^{+} fetal HSPCs while the proliferation of most control lines was only mildly affected by *TRIP13* loss (Fig. 2e). Gene expression profiling first confirmed that TRIP13 is upregulated as part of a fetal transcriptional program, being more highly expressed in fetal than in adult HSPCs and in pediatric AMKL compared to adult HSPCs and mature hematopoietic cells (Fig. 2f). Notably, NUP98::KDM5A expression further reinforced TRIP13 upregulation in fetal but not in adult cells, revealing a fetal context-specific effect of the fusion on TRIP13 (Fig. 2g).

Altogether, these data point to TRIP13 as a context-dependent vulnerability that is most evident in fetal-derived and NUP98::KDM5A-positive leukemias, thereby offering a potential target for therapeutic intervention in this high-risk AML subtype.

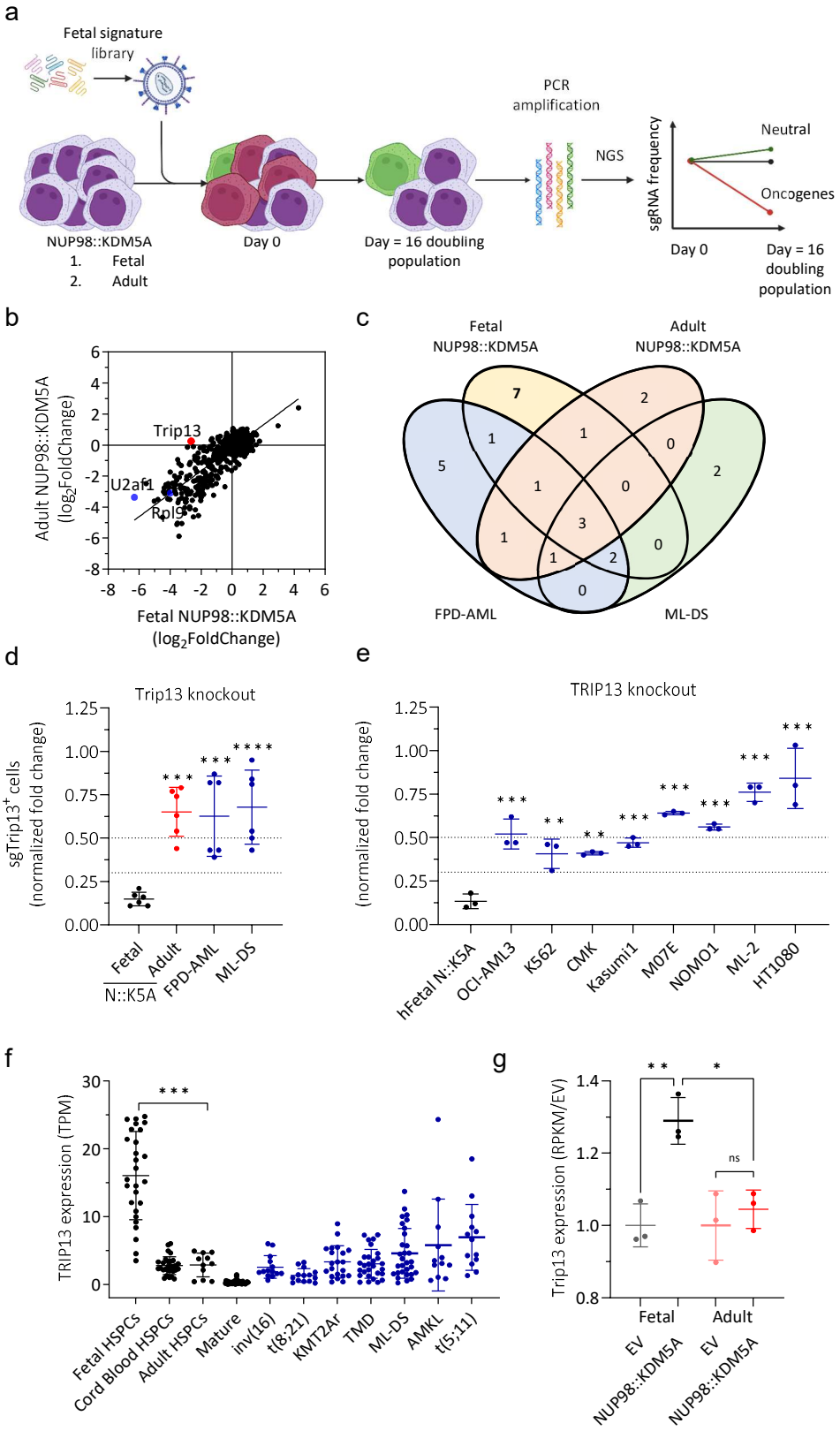

Fig. 2. CRISPR-Cas9 screen reveals *TRIP13* dependency in fetal NUP98::KDM5A⁺ model.

a) Schematic workflow of the high-throughput fetal signatures-based CRISPR-Cas9 *in vitro* screen.

b) Dot plots showing the log2 fold change of the fetal enriched genes targeted by sgRNAs in fetal (x-axis) and adult (y-axis) NUP98::KDM5A⁺ models. Blue dots represent positive control (*Rpl9*, *U2af1*). Red dots represent selected candidate gene *Trip13*. (n =2)

c) Venn diagram illustrating significantly ($P < 0.05$) depleted (depletion > 70%) sgRNAs in different murine leukemia models.
d) Dot plot showing the percentage of sgRNA-transduced (sgTrip13_1-3) fetal, adult NUP98::KDM5A$^+$ (N::K5A), FPD-AML and ML-DS models after 21 days of culture, normalized to (negative control sgRNA [sgCtr]) and to day 2 (mean ± s.d., n > 3 per sgRNA, 1-way ANOVA).
e) Dot plot showing the percentage of sgRNA-transduced (sgTrip13_1-3) hFL NUP98::KDM5A$^+$ cells and leukemia cell lines (OCI-AML3; K562; CMK; Kasumi1; M07E; NOMO1; ML-2) and non-leukemia cell line (HT1080) after 21 days of culture, normalized to (negative control sgRNA [sgCtr] and positive control sgRNA [sgRPL9 and sgU2AF1]) and to day 2 (mean ± s.d., n = 3 per sgRNA, 1-way ANOVA).
f) Dot plot showing the expression of *TRIP13* in subgroups of HSPCs and pediatric AML from the HemAtlas dataset.
g) Dot plot showing the expression of *Trip13* in control (EV) or NUP98::KDM5A$^+$ murine fetal and adult HSPCs cells after 2 weeks of culture (n = 3).

ns, not significant * $P < .05$, ** $P < .01$, ***$P < .001$, ****$P < .0001$.

Trip13 loss triggers TP53-dependent apoptosis

To verify that *Trip13* loss was causative for the observed phenotype, we co-transduced fetal NUP98::KDM5A$^+$ cells with *TRIP13* cDNA and *Trip13*-targeting sgRNAs. *TRIP13* overexpression fully rescued cell depletion, confirming on-target specificity (Fig. 3a). *Trip13* knockout, validated by Western blotting (Supplementary Fig. 3b), induced pronounced apoptosis (Fig. 3b) and a G_2/M arrest (Fig. 3c), consistent with TRIP13's role in mitotic checkpoint control [34], without altering differentiation status (Supplementary Fig. 3b).

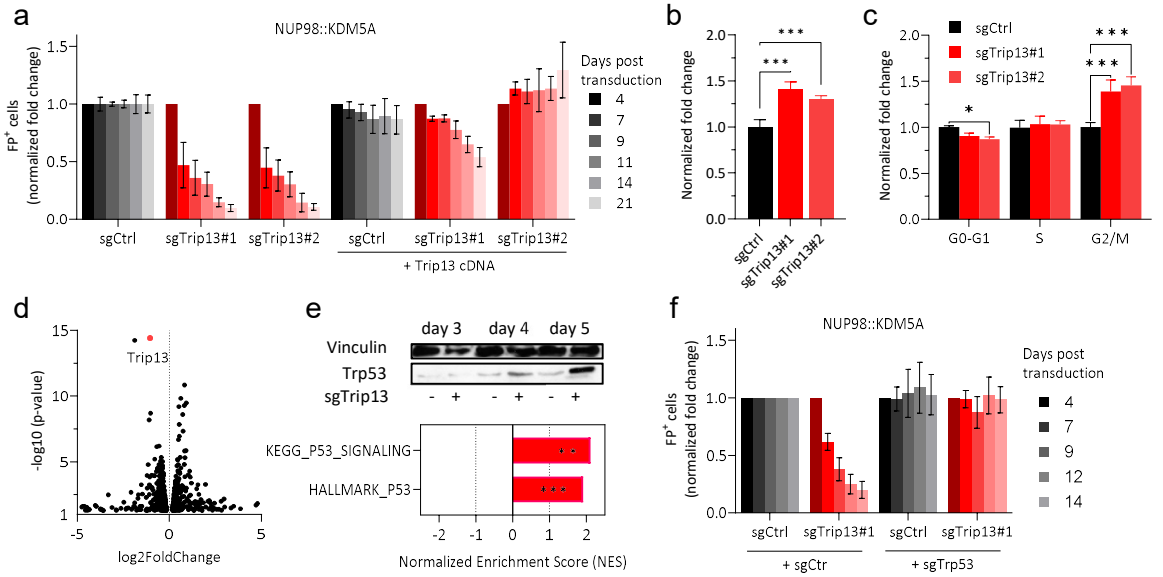

Fig. 3. Loss of *Trip13* promotes TP53 pathway activation and arrests fetal NUP98::KDM5A⁺ cell proliferation *in vitro*.

a) Bar plot showing the percentage of sgRNA-transduced (negative control sgRNA [sgCtr], sgTrip13#1-2) empty vector (EV) and TRIP13 overexpressing fetal NUP98::KDM5A⁺ cells after 14 days of culture, normalized to day 4 (mean±s.d., n > 3 per sgRNA, 1-way ANOVA)
b) Bar graphs showing the percentage of Annexin-V⁺ sgRNA-transduced (negative control sgRNA [sgCtr], sgTrip13#1-2) fetal NUP98::KDM5A⁺ cells after 5 days of culture, normalized to control sgRNA (sgCtr) (mean ± s.d., n > 3 per sgRNA, 1-way ANOVA).
c) Bar plot showing the percentage of sgRNA-transduced (negative control sgRNA [sgCtr], sgTrip13#1-2) fetal NUP98::KDM5A⁺ cells in G0-G1, S and G2/M phase after 5 days of culture (mean ± s.d., n > 3 per sgRNA, 2-way ANOVA).
d) Volcano plot showing the differentially expressed genes upon *Trip13* knocked out in fetal NUP98::KDM5A⁺ cells P-value < 0.05 (n = 3). RNA-seq-based gene expression analysis of sgRNA-transduced (negative control sgRNA [sgCtr], sgTrip13#1) fetal NUP98::KDM5A⁺ cells was performed after 4 days of culture.
e) Bar graphs showing the normalized enrichment scores (NES) of significantly deregulated gene sets associated with TP53 pathway in *Trip13* knocked out fetal NUP98::KDM5A⁺ cells compared to control sgRNA.
f) Timeline Western blot showing TP53 protein levels in sorted sgRNA-transduced (negative control sgRNA [Luc], sgTrip13#1) fetal NUP98::KDM5A⁺ cells 4 days after transduction. Endogenous Vinculin was used as loading control.
g) Bar plot showing the percentage of sgRNA-transduced (negative control sgRNA [sgCtr], sgTrip13, sgTrp53) fetal NUP98::KDM5A⁺ cells after 14 days of culture, normalized to day 4 (mean±s.d., n > 3 per sgRNA, 1-way ANOVA)

ns, not significant * P < .05, ** P < .01, ***P < .001, ****P < .0001.

Aiming for the molecular mechanisms underlying *Trip13* dependency, we measured gene expression changes 4 days post-gRNA transduction in fetal NUP98::KDM5A⁺ cells (Fig. 3d). Surprisingly, gene set enrichment analysis (GSEA [35]) revealed

perturbations only in the TP53 signaling pathway, which was positively enriched upon *Trip13* knock-out (Fig. 3e and Supplementary Fig. 3c, Supplementary Table 5). In line with this, TP53 protein levels were increased in a time-dependent manner upon *Trip13* knock-out (Fig. 3e), and co-deletion of *Trp53* completely rescued the growth defect induced by *Trip13* loss (Fig. 3f), demonstrating that TP53 activation mediates the *Trip13* dependency in fetal NUP98::KDM5A$^+$ AML cells. Several studies have shown that TRIP13 is involved in the regulation of DNA damage repair [36, 37]. To determine whether DNA damage contributes to TP53 activation and cell death, we measured γH2AX protein levels by Western blot. Although basal DNA damage was detected, *Trip13* deletion did not further increase γH2AX levels in fetal NUP98::KDM5A$^+$ cells versus controls (Supplementary Fig. 3d), suggesting that TP53 induction following *Trip13* loss occurred independently of additional genotoxic stress.

Together, these results establish that fetal *NUP98::KDM5A*$^+$ AML cells are sensitive to TP53 activation and that *Trip13* maintains leukemic survival by suppressing TP53, independently of DNA damage signaling.

TRIP13 interacts with PPM1D/WIP1 to repress TP53 pathway activation

To further understand how TRIP13 regulates TP53, we mapped its protein-protein interaction network via co-immunoprecipitation followed by mass spectrometry (IP-MS) using doxycycline-inducible hemagglutinin (HA)-tagged TRIP3 in a TP53 wild-type leukemia cell line (OCI-AML3) (Fig. 4a) [38, 39]. Among the proteins identified by TRIP13 pull-down, we focused on 33 candidates previously annotated in STRING as having functional or physical connection to TP53 (Fig. 4b). To investigate which of these candidate genes mediate the *Trip13*-dependency we used a functional approach. We hypothesized that the knock-out of a Trip13-interactor that is relevant for TP53 suppression would mimic the effect of *Trip13* knockout, thus leading to a

proliferative disadvantage in NUP98::KDM5A cells that is rescued by Trp53 co-deletion. Out of the 33 candidates, the knock-out of 16 Trip13-interactors caused a similar depletion rate as *Trip13* loss (Supplementary Fig. 4a). As *Trp53* knock-out rescues the effect of Trip13 loss, we next systematically combined *Trp53* knock-out with each of these 16 Trip13-interactors (Supplementary Fig. 4b). Upon Trp53 co-deletion, the protein phosphatase PPM1D/WIP1, a well-known regulator of TP53 in a direct and indirect manner via MDM2 stabilization, stood out as the top TRIP13 interactor (Fig. 4c and Supplementary Fig. 4b) [40]. Both *Trip13* and *Ppm1d* knock-out in fetal NUP98::KDM5A^{+} cells induced elevated TP53 protein levels (Fig. 4d). Co-immunoprecipitation of TRIP13 and Western blotting confirmed the TRIP13-PPM1D interaction in OCI-AML3 cells (Fig. 4e). Of note, *PPM1D/WIP1* expression – like TRIP13 – was elevated in pediatric AMKL patients compared to adult HSPCs and mature hematopoietic cells (Supplementary Fig. 4c).

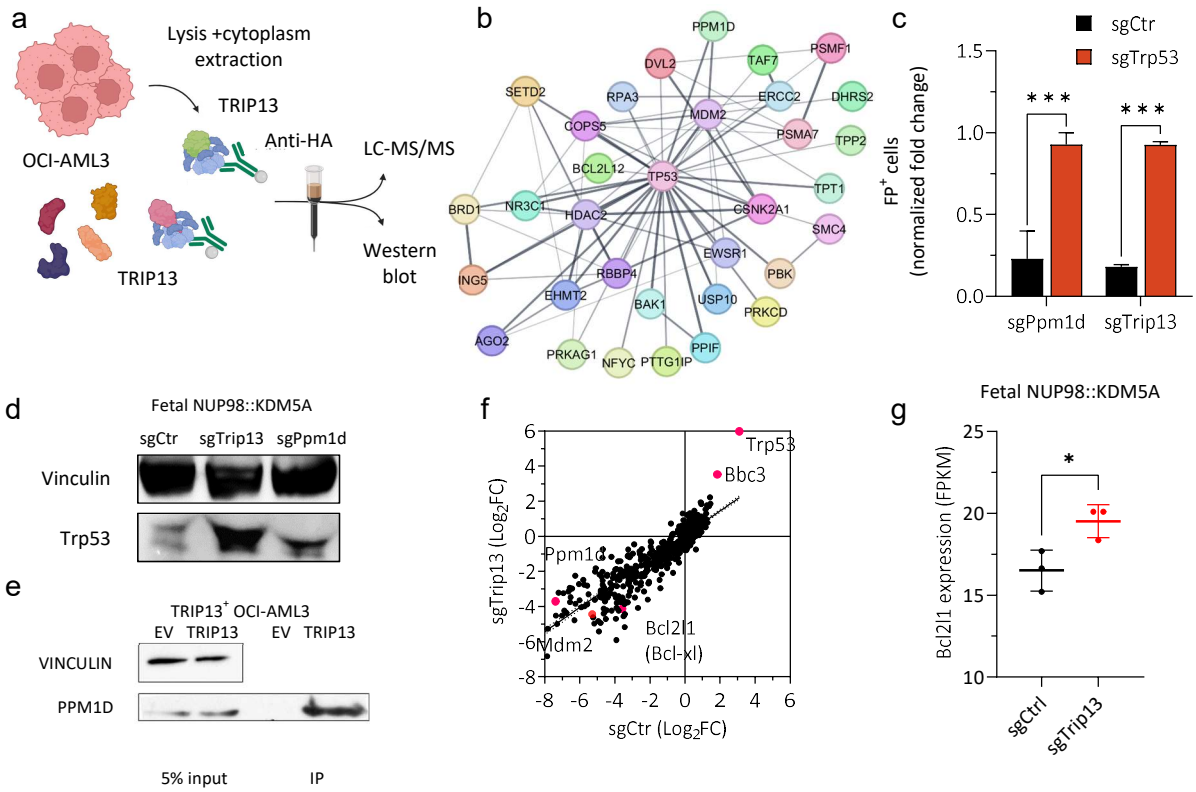

Fig. 4 TRIP13 interacts with PPM1D/WIP1 to repress TP53 pathway activation.

a) Experimental workflow for isolating HA-tagged TRIP13 protein and its interactors from OCI-AML3 cells.
b) String protein-protein interaction network of 33 TRIP13-interacting candidates. Network nodes (colored circles) represent proteins, lines between the nodes (edges) indicate the different types of interaction (functional and physical protein associations), the line thickness indicates the confidence of inter(0.4).
c) Bar plot showing the percentage of sgRNA-transduced [(sgPpm1d, sgTrip13) in combination with (negative control sgrna [sgCtr], sgTrp53)] fetal NUP98::KDM5A$^+$ cells after 14 days of culture, normalized to day 2 (mean±s.d., n > 3 per sgRNA, 1-way ANOVA)
d) Western blot showing TP53 protein levels in sorted sgRNA-transduced (negative control sgRNA [Luc], sgTrip13 and sgPpm1d) fetal NUP98::KDM5A$^+$ cells 4 days after transduction. Endogenous vinculin was used as loading control.
e) Western blot showing co-immunoprecipitation of Ppm1d with HA-tagged TRIP13 in OCI-AML3 cells. Endogenous vinculin was used as loading control.
f) Dot plots showing the log2 fold change of the TP53 pathway-related genes targeted by control (x-axis), *Trip13*-depleted (y-axis) fetal NUP98::KDM5A$^+$ cells. Red dots represent selected candidate genes (*Ppm1d*, *Mdm2*, *Bcl2l1*, *Bbc3*, *Trp53*). (n = 2)
g) Dot plot showing the expression of *Bcl2l1* of control or *Trip13*-depleted fetal NUP98::KDM5A$^+$ cells after 4 days of culture (n = 3).

ns, not significant * P < .05, ** P < .01, ***P < .001, ****P < .0001.

To gain more insights into the function of Trip13 in the TP53 signaling network, we performed a CRISPR-Cas9 knock-out screen of 704 TP53-pathway genes. in fetal NUP98::KDM5A$^+$ cells, with or without *Trip13* knockout (Fig. 4f). Ablation of Trp53 or Bbc3/Puma led to a strong enrichment of their corresponding sgRNAs in the CRISPR screen, indicating that mitochondrial apoptosis represents the predominant cell death mechanism induced upon Trip13 loss. Additionally, knock-out of *Mdm2* and *Bcl-xl/Bcl2l1* enhanced the antiproliferative effects of *Trip13* ablation, suggesting a potential therapeutic synergy (Fig. 4f). Notably, *Bcl-xl* and *Bbc3* expression was further elevated upon *Trip13* loss, indicating a feedback loop through which the cells attempt to evade apoptosis (Fig. 4g and Supplementary Fig. 4d).

Thus, our proteomic and function data show that TRIP13 binds to PPM1D, and both contribute to the suppression of TP53 activation in fetal NUP98::KDM5A$^+$ cells, which can be reversed by inhibiting MDM2 and BCL-XL.

Therapeutic Targeting of TRIP13 Reactivates TP53 in NUP98::KDM5A$^+$ AML

Our combined proteomic and genomic analyses identified TRIP13 as a critical suppressor of TP53 in fetal NUP98::KDM5A$^+$ AML, suggesting that pharmacological TRIP13 inhibition could be a therapeutic option. [41]

Treatment with the experimental small molecule TRIP13 inhibitor DCZ0415 replicated *Trip13* loss and robustly induced apoptosis in NUP98:KDM5A$^+$ cells in a dose-dependent manner (mean IC_{50} fetal = 22 µM, adult = 26 µM). NUP98::KDM5A cells were significantly more sensitive than FPD-AML, ML-DS or mBM-HSPC cells (mean IC_{50}: FPD-AML: 50 µM, ML-DS: 35 µM, mBM-HSPCs: 45 µM) (Fig. 5a and Supplementary Fig. 5a-b). Human fetal NUP98::KDM5A$^+$ cells were similarly sensitive to DCZ0415 (mean IC_{50} = 19 µM), while OCI-AML3, Kasumi1 or M07E showed lower or only partial response (IC_{50}: OCI-AML3: 32 µM, Kasumi-1/M07e: NM = not measurable; Fig. 5b and Supplementary Fig. 5c). DCZ0415 treatment caused activation of the TP53 pathway and induced cell death, which could be rescued both by overexpressing TRIP13 or by knocking out *Trp53* (Fig. 5c and Supplementary Fig. 5d).

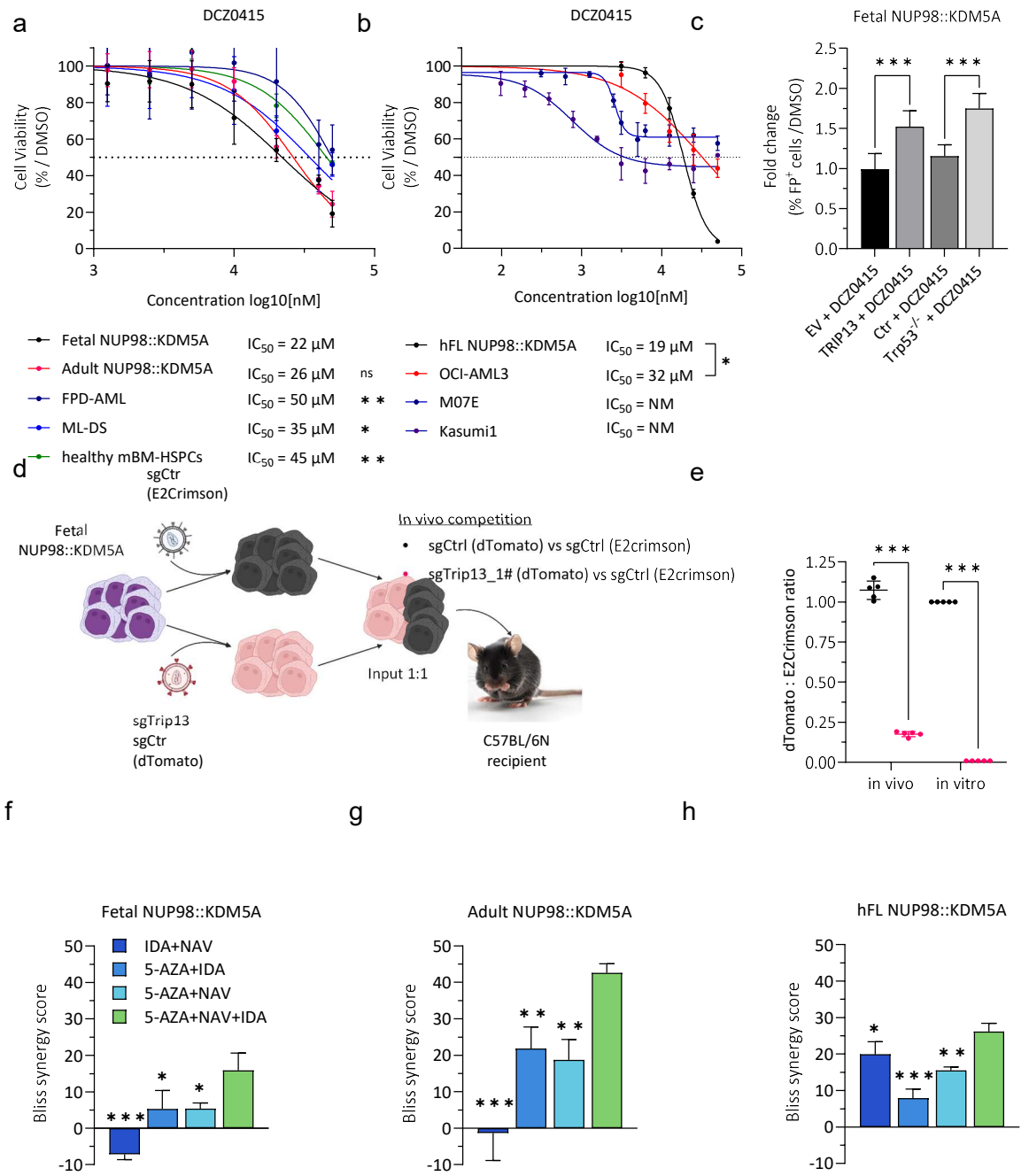

Fig. 5. Pharmacological inhibition of TRIP13 as a therapeutic strategy in NUP98::KDM5A⁺ pediatric leukemia.

a) Dose-response curves for DCZ0415 (TRIP13 inhibitor) in fetal and adult NUP98::KDM5A⁺, ML-DS and FPD-AML models and healthy mBM-HSPCs after 5 days of treatment *in vitro*. The corresponding IC_{50}-values are depicted below the graphs. (mean ± s.d. , n > 3, 1-way ANOVA)

b) Dose-response curves for DCZ0415 (TRIP13 inhibitor) in hFL NUP98::KDM5A⁺ cells and OCI-AML3, M07E and Kasumi1 after 5 days of treatment *in vitro*. The corresponding IC_{50}-values are depicted below the graphs. (mean ± s.d. , n > 3, 1-way ANOVA).

c) Bar graphs showing the percentage of sgRNA-transduced (negative control sgRNA [sgCtr], sgTrp53) and empty vector (EV) or TRIP13-overexpressing fetal NUP98::KDM5A⁺ cells after 7 days of treatment with DCZ0415 (TRIP13 inhibitor) *in vitro*. (mean±s.d. , n > 3, 1-way ANOVA).

d) Experimental setup for evaluating the genetic ablation of *Trip13* in fetal NUP98::KDM5A$^+$ cells *in vivo*. Fetal NUP98::KDM5A$^+$ cells (with stable Cas9 expression) were transduced with sgTrip13 (dTomato) and sgCtr (dTomato) and mixed 1:1 with sgCtr (E2Crimson), before transplantation into sublethally irradiated recipient mice.
e) Dot plot showing the ratio of dTomato$^+$ to E2Crimson$^+$ cells in the bone marrow of mice euthanized 4 weeks after transplantation (n = 5, 2-way ANOVA) and after 4 weeks of culture, normalized to day 0 (n = 3, 2-way ANOVA)
f) Bar plot showing the summary Bliss synergy score of double or triple combinatorial treatment with drugs (IDA = Idasanutlin, NAV = Navitoclax, 5-AZA = 5-Azacytidine) of fetal NUP98::KDM5A$^+$ cells after 5 days. (mean ± s.d. , n = 3, 1-way ANOVA related to the triple combination)
g) Bar plot showing the summary Bliss synergy score of double or triple combinatorial treatment with drugs (IDA = Idasanutlin, NAV = Navitoclax, 5-AZA = 5-Azacytidine) of adult NUP98::KDM5A$^+$ cells after 5 days. (mean ± s.d. , n = 3, 1-way ANOVA related to the triple combination)
h) Bar plot showing the summary Bliss synergy score of double or triple combinatorial treatment with drugs (IDA = Idasanutlin, NAV = Navitoclax, 5-AZA = 5-Azacytidine) of hFL NUP98::KDM5A$^+$ cells after 5 days. (mean ± s.d. , n >=3, 1-way ANOVA related to the triple combination)

ns, not significant * P < .05, ** P < .01, ***P < .001, ****P < .0001.

Lastly, we evaluated Trip13 knock-out *in vivo* through fluorescence-based competitive transplantation assays using fetal NUP98::KDM5A$^+$ cells (Fig. 5d). Trip13-depleted leukemic blasts were significantly diminished in the bone marrow of recipient mice at the experimental endpoint (Fig. 5e), consistent with *in vitro* findings (Fig. 5e).

These results establish that TRIP13 inhibition predominantly affects NUP98::KDM5A$^+$ leukemic cell survival by reactivating TP53 signaling, supporting its development as a targeted therapeutic strategy for this high-risk pediatric AML subtype.

A clinically applicable intervention exploiting TP53 sensitivity in NUP98::KDM5A-driven AML

As TRIP13 inhibitors are still in early development, thus prohibiting clinical translation at this stage [42, 43], we sought to pharmacologically mimic TRIP13 loss using TP53-reactivating drugs that are approved or in late-stage clinical trials. Our TP53 pathway CRISPR screening suggested MDM2 and BCL2L1 as promising candidates (Fig. 4f). The MDM2 inhibitor idasanutlin [44] induced dose-dependent apoptosis in both fetal and adult NUP98::KDM5A$^+$ cells, whereas the BCL2/BCL-XL inhibitor navitoclax [45,

46] was active only in fetal cells, with partial effects in adult NUP98::KDM5A$^+$, FPD-AML, and ML-DS models (Supplementary Fig. 5e-g-h).

Consequently, we performed combined treatment with Idasanutlin and Navitoclax but could not detect any synergistic activity (Fig. 5f-h). Notably, combined treatment with DCZ0415 and Idasanutlin or Navitoclax resulted in synergistic killing in fetal NUP98::KDM5A$^+$ cells (Supplementary Fig. 5i), indicating that additional triggers are needed to mimic the effect of TRIP13 inhibition. Given the established role of hypomethylating agents as a chemotherapy sensitizer [47-49], we incorporated 5-azacytidine (5-Aza) into the idasanutlin-navitoclax regimen. This triple combination produced robust synergy in fetal, adult, and human fetal NUP98::KDM5A$^+$ cells (Bliss synergy scores: 16, 43, and 26, respectively) and was broadly active across models (Fig. 5f-h).

Hence, our clinically applicable strategy for TP53 reactivation, using a combination of FDA-approved drugs Idasanutlin and 5-Azacytidine along with the investigational agent Navitoclax, offers promising therapeutic strategies for rapid translation into early-phase trials in NUP98::KDM5A$^+$ AML.

Discussion

In this study, we identified a novel therapeutic vulnerability in infant leukemia by interrogating the developmental basis of the disease, moving beyond an oncogene-centric framework. This ontogeny-focused approach revealed a targetable dependency linked to fetal hematopoiesis and may represent a paradigm shift for other malignancies with marked developmental origin. NUP98::KDM5A-rearranged AML is a rare but highly aggressive subtype that occurs predominantly in infants and very young children below the age of 2 years [6-8]. Its early occurrence strongly suggests

that leukemia initiates during embryogenesis [50] , implicating the unique biology of fetal hematopoiesis in disease development. Even with intensive chemotherapy and allogeneic hematopoietic stem cell transplantation (HSCT), outcomes remain poor, relapses are frequent and high treatment-related morbidity is observed. Achieving deep, MRD-negative remissions prior to HSCT is a critical determinant of long-term survival, yet current induction regimens are often too toxic or ineffective for this fragile patient population [51].

While ontogeny has increasingly gained recognition in other pediatric hematologic malignancies, including CBFA2T3::GLIS2 and KMT2A-rearranged leukemias [6], its impact in NUP98::KDM5A-driven AML has not been directly addressed. Using matched fetal and adult HSPC models, we demonstrate that NUP98::KDM5A-driven AML arising in a fetal context is more aggressive and retains ontogeny-specific transcriptional programs [19, 20, 52]. Functional genomic interrogation of fetal-enriched genes identified TRIP13 – a AAA^+ ATPase and direct interactor of the TP53 phosphatase PPM1D/WIP1 – as a critical dependency in fetal NUP98::KDM5A$^+$ cells. TRIP13 suppresses TP53 activation, and its loss or inhibition reactivates TP53 signaling, triggering G_2/M arrest and mitochondrial apoptosis without additional DNA damage [34, 36]. Our findings suggest that TRIP13 mitigates NUP98::KDM5A-induced DNA stress [53] by modulating TP53 activity, potentially by its physical interaction with PPM1D, a well-established oncogenic suppressor of TP53 [54]. The precise mechanism by which TRIP13 may regulate PPM1D activity remains to be defined. Given that TRIP13 has been reported to remodel protein conformation through its ATPase function [55], it is plausible that TRIP13 similarly modulates PPM1D conformation to influence its phosphatase activity. Mechanistically, this positions TP53 repression via TRIP13/PPM1D at the core of leukemic maintenance and links it to the

oncofetal transcriptional programs induced -at least partially- by NUP98::KDM5A [53, 56].

While we cannot yet determine whether these programs reflect direct binding of NUP98::KDM5A to oncofetal genes or secondary downstream effects, a recent study found developmental and oncofetal genes such as *Nkx2-3* and *Igf2bp3* as direct targets of NUP98::KDM5A, supporting our hypothesis of a direct role of NUP98::KDM5A in fetal gene activation [53]**.**

Prior mechanistic studies of NUP98::KDM5A-driven leukemia have uncovered dependencies such as the MEN–KMT2A axis, CDK6, and CDK12 [52, 53, 56] , all of which converge on sustaining active transcription and cell-cycle progression.

Such enforced proliferation and DNA replication intrinsically promote DNA damage [57], consistent with reports that NUP98::KDM5A-expressing cells exhibit high levels of DNA repair machinery, baseline DNA damage, and heightened sensitivity to CDK12/13 inhibition [53, 58]. Coping with this DNA stress and avoiding apoptosis appears to be a central requirement of transformation, which we show involves TRIP13 acting through PPM1D to maintains low levels of TP53. Notably, the DNA damage–related genes identified in our CRISPR–Cas9 screens were also reported by Troester et al. [53] as maintained by *NUP98::KDM5A* and are upregulated during fetal development, further aligning our findings with theirs. While PPM1D is the prime TP53-modulating factor interacting with TRIP13 in our system, our protein-protein interaction analysis revealed numerous additional TP53 network components interacting with TRIP13, including 16 candidates whose perturbation partially phenocopied the TP53-dependent depletion seen upon Trip13 loss. This multimodal regulation likely explains the higher TP53 levels in *Trip13* knock-out compared to *Ppm1d* knock-out cells, underscoring the complexity of TRIP13-mediated TP53 control.

Importantly, our work provides proof-of-concept for pharmacologic inhibition of TRIP13 using the small-molecule inhibitor DCZ0415, which faithfully recapitulated the effects of genetic TRIP13 loss, inducing TP53-dependent apoptosis in NUP98::KDM5A^{+} AML cells. Although DCZ0415 is not yet clinically deployable, these findings underscore the potential of TRIP13 as a druggable target in high-risk pediatric AML and warrant the development of next-generation inhibitors suitable for clinical testing.

To bridge the gap until such agents become available, our TP53-pathway CRISPR screen identified MDM2 and BCL2L1 (BCL-XL) as actionable co-targets [59].

Unpublished work from our lab and a previous work also demonstrated a molecular dependency on BCL-XL and resistance to BCL2-inhibition (data not shown) in AMKL, in particular in the presence of CBFA2T3::GLIS2 translocation [60]. Our results validate and extend these findings to other fusions, including NUP98-translocated pediatric leukemia, while the loss of BBC3 and TP53 expectedly counteracts this mechanism [61, 62]. Guided by these insights, we designed a triple combination of idasanutlin (MDM2 inhibitor), navitoclax (BCL2/BCL-XL inhibitor), and 5-azacytidine (hypomethylating sensitizer [63]). This regimen phenocopied TRIP13 loss and triggered robust, synergistic apoptosis across fetal, adult, and human fetal NUP98::KDM5A^{+} AML cells. Importantly, all three agents are FDA-approved or in advanced clinical testing, enabling rapid translational potential.

Comparative studies in established murine AML models [31] revealed that, while this pharmacologic strategy exhibited broader activity and less specificity than TRIP13 depletion, it nonetheless produced potent antileukemic effects. This difference likely reflects non-identical mechanisms of TP53 engagement by idasanutlin versus TRIP13 inhibition, consistent with the observed synergy between both approaches. From a therapeutic standpoint, such broader activity may represent an advantage, potentially

extending benefit beyond NUP98-rearranged disease to other pediatric and adult AML subtypes, though further validation is needed.

Clinically, this mechanism-based regimen could serve as an induction or re-induction strategy to achieve deep remission without the toxicity of additional intensive chemotherapy. Reactivating TP53 and priming apoptosis could promote an optimal remission status before HSCT, offering a tangible opportunity to improve cure rates in NUP98::KDM5A-driven AML. By enhancing both disease clearance and pre-transplant fitness, this strategy could improve HSCT outcomes in a population with otherwise dismal survival rates.

Current treatment paradigms for high risk, relapsed or refractory pediatric AML – particularly in infants – rely on intensified cytarabine- or fludarabine-based chemotherapy, often combined with anthracyclines or narrow-spectrum targeted agents [64]. While these regimens can achieve remission, they do so with substantial toxicity, prolonged myelosuppression, and high treatment-related morbidity, frequently delaying or precluding HSCT. In contrast, therapeutic strategies targeting the TRIP13-TP53-axis directly with novel TRIP13 inhibitors, or indirectly through the idasanutlin–navitoclax–5-azacytidine combination, offer a targeted, potentially less intensive yet mechanistically potent alternative, distinct from other novel approaches such as those targeting the Menin–KMT2A axis [52, 53, 56]. Reactivating TP53 and priming apoptosis could promote an optimal remission status before HSCT, offering a tangible opportunity to improve cure rates in NUP98::KDM5A-driven AML.

More broadly, our work illustrates how systematic functional interrogation of ontogeny-specific programs can uncover lineage- and age-dependent vulnerabilities invisible to purely mutation-focused analyses. In NUP98::KDM5A^{+} AML, this strategy exposed a central TRIP13/PPM1D–TP53 survival axis, validated TRIP13 as a direct therapeutic target, and delivered an immediately translatable combination regimen that mimics its

inhibition. This paradigm – leveraging developmental biology to expose unique, druggable dependencies – may prove transformative for other aggressive pediatric cancers with developmental origins.

References

1. Bolouri, H., et al., *The molecular landscape of pediatric acute myeloid leukemia reveals recurrent structural alterations and age-specific mutational interactions.* Nat Med, 2018. **24**(1): p. 103-112.
2. Papaemmanuil, E., et al., *Genomic Classification and Prognosis in Acute Myeloid Leukemia.* N Engl J Med, 2016. **374**(23): p. 2209-2221.
3. Marceau-Renaut, A., et al., *Molecular Profiling Defines Distinct Prognostic Subgroups in Childhood AML: A Report From the French ELAM02 Study Group.* Hemasphere, 2018. **2**(1): p. e31.
4. Reinhardt, D., E. Antoniou, and K. Waack, *Pediatric Acute Myeloid Leukemia-Past, Present, and Future.* J Clin Med, 2022. **11**(3).
5. Elgarten, C.W. and R. Aplenc, *Pediatric acute myeloid leukemia: updates on biology, risk stratification, and therapy.* Current Opinion in Pediatrics, 2020. **32**(1): p. 57-66.
6. Lopez, C.K., et al., *Ontogenic Changes in Hematopoietic Hierarchy Determine Pediatric Specificity and Disease Phenotype in Fusion Oncogene-Driven Myeloid Leukemia.* Cancer Discov, 2019. **9**(12): p. 1736-1753.
7. Okeyo-Owuor, T., et al., *The efficiency of murine MLL-ENL-driven leukemia initiation changes with age and peaks during neonatal development.* Blood Adv, 2019. **3**(15): p. 2388-2399.
8. Calvi, L.M. and D.C. Link, *The hematopoietic stem cell niche in homeostasis and disease.* Blood, 2015. **126**(22): p. 2443-51.
9. Mack, R., et al., *The Fetal-to-Adult Hematopoietic Stem Cell Transition and its Role in Childhood Hematopoietic Malignancies.* Stem Cell Rev Rep, 2021. **17**(6): p. 2059-2080.
10. de Smith, A.J. and L.G. Spector, *In Utero Origins of Acute Leukemia in Children.* Biomedicines, 2024. **12**(1).
11. Gruber, T.A. and J.R. Downing, *The biology of pediatric acute megakaryoblastic leukemia.* Blood, 2015. **126**(8): p. 943-9.
12. de Rooij, J.D., et al., *Pediatric non-Down syndrome acute megakaryoblastic leukemia is characterized by distinct genomic subsets with varying outcomes.* Nat Genet, 2017. **49**(3): p. 451-456.
13. de Rooij, J.D., et al., *Recurrent abnormalities can be used for risk group stratification in pediatric AMKL: a retrospective intergroup study.* Blood, 2016. **127**(26): p. 3424-30.
14. Gough, S.M., C.I. Slape, and P.D. Aplan, *NUP98 gene fusions and hematopoietic malignancies: common themes and new biologic insights.* Blood, 2011. **118**(24): p. 6247-57.
15. Bertrums, E.J.M., et al., *Comprehensive molecular and clinical characterization of NUP98 fusions in pediatric acute myeloid leukemia.* Haematologica, 2023.
16. Gough, S.M., et al., *NUP98-PHF23 is a chromatin-modifying oncoprotein that causes a wide array of leukemias sensitive to inhibition of PHD histone reader function.* Cancer Discov, 2014. **4**(5): p. 564-77.
17. Wang, G.G., et al., *Haematopoietic malignancies caused by dysregulation of a chromatin-binding PHD finger.* Nature, 2009. **459**(7248): p. 847-51.
18. Wang, G.G., et al., *NUP98-NSD1 links H3K36 methylation to Hox-A gene activation and leukaemogenesis.* Nat Cell Biol, 2007. **9**(7): p. 804-12.
19. Roy, A., et al., *Transitions in lineage specification and gene regulatory networks in hematopoietic stem/progenitor cells over human development.* Cell Rep, 2021. **36**(11): p. 109698.
20. Ivanovs, A., et al., *Human haematopoietic stem cell development: from the embryo to the dish.* Development, 2017. **144**(13): p. 2323-2337.
21. Popescu, D.M., et al., *Decoding human fetal liver haematopoiesis.* Nature, 2019. **574**(7778): p. 365-371.
22. Bowie, M.B., et al., *Identification of a new intrinsically timed developmental checkpoint that reprograms key hematopoietic stem cell properties.* Proc Natl Acad Sci U S A, 2007. **104**(14): p. 5878-82.

23. Ranzoni, A.M., et al., *Integrative Single-Cell RNA-Seq and ATAC-Seq Analysis of Human Developmental Hematopoiesis.* Cell Stem Cell, 2021. **28**(3): p. 472-487.e7.
24. Michmerhuizen, N.L., J.M. Klco, and C.G. Mullighan, *Mechanistic insights and potential therapeutic approaches for NUP98-rearranged hematologic malignancies.* Blood, 2020. **136**(20): p. 2275-2289.
25. de Rooij, J.D., et al., *NUP98/JARID1A is a novel recurrent abnormality in pediatric acute megakaryoblastic leukemia with a distinct HOX gene expression pattern.* Leukemia, 2013. **27**(12): p. 2280-8.
26. Newman, A.M., et al., *Determining cell type abundance and expression from bulk tissues with digital cytometry.* Nat Biotechnol, 2019. **37**(7): p. 773-782.
27. Dahlin, J.S., et al., *A single-cell hematopoietic landscape resolves 8 lineage trajectories and defects in Kit mutant mice.* Blood, 2018. **131**(21): p. e1-e11.
28. Noort, S., et al., *The clinical and biological characteristics of NUP98-KDM5A in pediatric acute myeloid leukemia.* Haematologica, 2021. **106**(2): p. 630-634.
29. Schwarzer, A., et al., *The non-coding RNA landscape of human hematopoiesis and leukemia.* Nat Commun, 2017. **8**(1): p. 218.
30. Förster, A., et al., *Beyond Pathogenic RUNX1 Germline Variants: The Spectrum of Somatic Alterations in RUNX1-Familial Platelet Disorder with Predisposition to Hematologic Malignancies.* Cancers (Basel), 2022. **14**(14).
31. Labuhn, M., et al., *Mechanisms of Progression of Myeloid Preleukemia to Transformed Myeloid Leukemia in Children with Down Syndrome.* Cancer Cell, 2019. **36**(2): p. 123-138.e10.
32. Grimm, J., D. Heckl, and J.H. Klusmann, *Molecular Mechanisms of the Genetic Predisposition to Acute Megakaryoblastic Leukemia in Infants With Down Syndrome.* Front Oncol, 2021. **11**: p. 636633.
33. Gialesaki, S., et al., *RUNX1 isoform disequilibrium promotes the development of trisomy 21–associated myeloid leukemia.* Blood, 2023. **141**(10): p. 1105-1118.
34. Vader, G., *Pch2TRIP13: controlling cell division through regulation of HORMA domains.* Chromosoma, 2015. **124**(3): p. 333-339.
35. Subramanian, A., et al., *Gene set enrichment analysis: A knowledge-based approach for interpreting genome-wide expression profiles.* Proceedings of the National Academy of Sciences, 2005. **102**(43): p. 15545-15550.
36. Banerjee, R., et al., *TRIP13 promotes error-prone nonhomologous end joining and induces chemoresistance in head and neck cancer.* Nat Commun, 2014. **5**: p. 4527.
37. Jeong, H., et al., *TRIP13 Participates in Immediate-Early Sensing of DNA Strand Breaks and ATM Signaling Amplification through MRE11.* Cells, 2022. **11**(24).
38. Sullivan, K.D., et al., *Mechanisms of transcriptional regulation by p53.* Cell Death & Differentiation, 2018. **25**(1): p. 133-143.
39. Kruse, J.-P. and W. Gu, *Modes of p53 Regulation.* Cell, 2009. **137**(4): p. 609-622.
40. Andrysik, Z., et al., *PPM1D suppresses p53-dependent transactivation and cell death by inhibiting the Integrated Stress Response.* Nat Commun, 2022. **13**(1): p. 7400.
41. Wang, Y., et al., *A Small-Molecule Inhibitor Targeting TRIP13 Suppresses Multiple Myeloma Progression.* Cancer Res, 2020. **80**(3): p. 536-548.
42. Agarwal, S., et al., *DCZ0415, a small-molecule inhibitor targeting TRIP13, inhibits EMT and metastasis via inactivation of the FGFR4/STAT3 axis and the Wnt/β-catenin pathway in colorectal cancer.* Mol Oncol, 2022. **16**(8): p. 1728-1745.
43. Dong, S., et al., *Design and synthesis of cantharidin derivative DCZ5418 as a TRIP13 inhibitor with anti-multiple myeloma activity in vitro and in vivo.* Bioorg Med Chem Lett, 2024. **98**: p. 129590.
44. Konopleva, M., et al., *MDM2 inhibition: an important step forward in cancer therapy.* Leukemia, 2020. **34**(11): p. 2858-2874.
45. Afreen, S., et al., *BCL-XL expression is essential for human erythropoiesis and engraftment of hematopoietic stem cells.* Cell Death Dis, 2020. **11**(1): p. 8.

46. Pullarkat, V.A., et al., *Venetoclax and Navitoclax in Combination with Chemotherapy in Patients with Relapsed or Refractory Acute Lymphoblastic Leukemia and Lymphoblastic Lymphoma.* Cancer Discov, 2021. **11**(6): p. 1440-1453.
47. Straube, J., S.W. Lane, and T. Vu, *Optimizing DNA hypomethylating therapy in acute myeloid leukemia and myelodysplastic syndromes.* Bioessays, 2021. **43**(10): p. e2100125.
48. Maslah, N., et al., *Niclosamide combined to Azacitidine to target TP53-mutated MDS/AML cells.* Leukemia, 2024. **38**(7): p. 1630-1633.
49. DiNardo, C.D., et al., *Phase 1 dose escalation study of the MDM2 inhibitor milademetan as monotherapy and in combination with azacitidine in patients with myeloid malignancies.* Cancer Med, 2024. **13**(14): p. e70028.
50. Cazzola, A., et al., *Prenatal Origin of Pediatric Leukemia: Lessons From Hematopoietic Development.* Front Cell Dev Biol, 2020. **8**: p. 618164.
51. Rettinger, E., et al., *The hallmarks of hematopoietic stem cell transplantation for pediatric acute myeloid leukemia.* Leukemia, 2025.
52. Heikamp, E.B., et al., *The menin-MLL1 interaction is a molecular dependency in NUP98-rearranged AML.* Blood, 2022. **139**(6): p. 894-906.
53. Troester, S., et al., *Transcriptional and epigenetic rewiring by the NUP98::KDM5A fusion oncoprotein directly activates CDK12.* Nat Commun, 2025. **16**(1): p. 4656.
54. Ogasawara, S., et al., *Novel inhibitors targeting PPM1D phosphatase potently suppress cancer cell proliferation.* Bioorg Med Chem, 2015. **23**(19): p. 6246-9.
55. Mapelli, M. and A. Musacchio, *MAD contortions: conformational dimerization boosts spindle checkpoint signaling.* Curr Opin Struct Biol, 2007. **17**(6): p. 716-25.
56. Schmoellerl, J., et al., *CDK6 is an essential direct target of NUP98 fusion proteins in acute myeloid leukemia.* Blood, 2020. **136**(4): p. 387-400.
57. Shimura, T., et al., *Cyclin D1 overexpression perturbs DNA replication and induces replication-associated DNA double-strand breaks in acquired radioresistant cells.* Cell Cycle, 2013. **12**(5): p. 773-82.
58. Domingo-Reinés, J., et al., *The pediatric leukemia oncoprotein NUP98-KDM5A induces genomic instability that may facilitate malignant transformation.* Cell Death Dis, 2023. **14**(6): p. 357.
59. Bell, H.L., et al., *Combination p53 activation and BCL-xL/BCL-2 inhibition as a therapeutic strategy in high-risk and relapsed acute lymphoblastic leukemia.* Leukemia, 2024. **38**(6): p. 1223-1235.
60. Gress, V., et al., *CBFA2T3::GLIS2 pediatric acute megakaryoblastic leukemia is sensitive to BCL-XL inhibition by navitoclax and DT2216.* Blood Adv, 2024. **8**(1): p. 112-129.
61. Nechiporuk, T., et al., *The TP53 Apoptotic Network Is a Primary Mediator of Resistance to BCL2 Inhibition in AML Cells.* Cancer Discov, 2019. **9**(7): p. 910-925.
62. Pan, R., et al., *Synthetic Lethality of Combined Bcl-2 Inhibition and p53 Activation in AML: Mechanisms and Superior Antileukemic Efficacy.* Cancer Cell, 2017. **32**(6): p. 748-760.e6.
63. Kiziltepe, T., et al., *5-Azacytidine, a DNA methyltransferase inhibitor, induces ATR-mediated DNA double-strand break responses, apoptosis, and synergistic cytotoxicity with doxorubicin and bortezomib against multiple myeloma cells.* Mol Cancer Ther, 2007. **6**(6): p. 1718-27.
64. Conneely, S.E. and A.M. Stevens, *Acute Myeloid Leukemia in Children: Emerging Paradigms in Genetics and New Approaches to Therapy.* Curr Oncol Rep, 2021. **23**(2): p. 16.

Contributions

L.N.C performed experiments, analyzed and interpreted the data, and wrote the manuscript; L.P., H.I., and C.I. performed experiments, analyzed the data, and revised the manuscript; K.S. performed bioinformatics analysis and revised the manuscript;

K.M., and L.G. performed experiments; M.V. revised the manuscript; A.S. supervised the analyses and revised the manuscript; J.-H.K. and D.H. designed the study, analyzed and interpreted the data, wrote the manuscript, and academically drove the project.

Acknowledgments

The authors thank D. Trono of EPFL (Lausanne, Switzerland), for kindly providing both pMD2.G (plasmid 12259; Addgene) and psPAX2 (plasmid 12260; Addgene); A. Santos (University of Halle-Wittenberg) for assistance with flow cytometry; and K. Huke for assistance with animal experiments.

L.N.C, M.V., and D.H. were supported by the Frankfurt Foundation for Children with Cancer. This work was supported by the German José Carreras Leukemia Foundation (DJCLS 12 R/2024) and by grants from the parents Association “Hilfe für Krebskranke Kinder e.V.” (L.N.C, J.-H.K. and D.H).

Illustrations (Figures 1a, 2a, 4a and 5d and graphical abstract) were created with BioRender.com.